frontiers | Frontiers in Marine Science

TYPE Original Research
PUBLISHED 02 May 2025
DOI 10.3389/fmars.2025.1553799

OPEN ACCESS

EDITED BY
Hongjian Zhu,
Yanshan University, China

REVIEWED BY
Yazhou Liu,
China University of Petroleum, China
Jin Xiao,
China Geological Survey, China
Qin Zhang,
Delft University of Technology, Netherlands

*CORRESPONDENCE
Qianru Wang
qianru.wang@cug.edu.cn

RECEIVED 31 December 2024
ACCEPTED 09 April 2025
PUBLISHED 02 May 2025

CITATION
Wang Q, Huang H and Jiang T (2025) Instantaneous petroleum charge in the Shunbei reservoirs, Tarim Basin.
Front. Mar. Sci. 12:1553799.
doi: 10.3389/fmars.2025.1553799

Instantaneous petroleum charge in the Shunbei reservoirs, Tarim Basin

Qianru Wang[1]*, Haiping Huang[2] and Tao Jiang[1]

[1]Hubei Key Laboratory of Marine Geological Resources, China University of Geosciences, Wuhan, China, [2]Department of Earth, Energy, and Environment, University of Calgary, Calgary, AB, Canada

Instantaneous petroleum charge is uncommon in sedimentary basins, particularly in the Tarim Basin, where petroleum has accumulated from multiple source rocks with multiple episode charge stages. In the present study, an instantaneous petroleum charge was identified within the No.3 fault zone of the Shunbei reservoirs in the Tarim Basin. The oil from Well Shunbei 3 (SHB3 oil) is considered as an end member close to the stratigraphic maturity of source rock at a certain maturity level with evidence from *n*-alkanes, isoprenoids, steroids, terpenoids, diamondoids and a series of aromatic hydrocarbons. In comparison to oil samples from the No.1 fault zone, SHB3 oil did not receive the early-charged oil whereas it has not undergone petroleum charging during the very late maturation stages. The end member of instantaneous petroleum charge in Shunbei reservoirs provides valuable insights into petroleum generation, expulsion and charge histories of ultra-deep Ordovician reservoirs in the Tarim Basin.

KEYWORDS

thermal maturity, biomarkers, instantaneous petroleum charge, Shunbei reservoirs, Tarim Basin

1 Introduction

Petroleum in reservoirs (hereafter referred to as reservoired petroleum) typically contains a complex mixture of varying maturities due to the intricate processes of petroleum generation and accumulation. Petroleum generation, as widely recognized, involves the transformation of solid organic matter within source rocks into liquid or gaseous hydrocarbons through temperature-induced processes (Tissot et al., 1987). According to Huang et al. (2022), the entire petroleum generation process within a suit of source rock might span a few million years or a few tens of millions of years given the geological heating rates of 1–10°C/My for a typical petroleum system. As the maturity of source rocks increases over geological time or burial depth, the expelled petroleum charging into the reservoir is more and more mature provided there is no interruption. However, it is common that petroleum from multiple source rocks could accumulate into the same reservoir with multiple episode charge stages in sedimentary basins. Additionally,

secondary alterations, such as biodegradation, thermochemical sulfate reduction (TSR), evaporative fractionation and thermal cracking, can modify the original petroleum compositions (Larter and Aplin, 1995; Horstad and Larter, 1997; Wilhelms and Larter, 2004; Lerch et al., 2016).

Thermal maturity refers to the degree of petroleum generation from source rocks over a geological timescale, a concept often described as "kinetic maturity" (Ungerer and Pelet, 1987). While source rocks and oils are two commonly objects for thermal maturity assessment, they represent distinct maturity concepts. The maturity of source rocks is typically determined by vitrinite reflectance on organic-rich sediments using petrography-based methods. This can be referred to as "stratigraphic maturity" (Huang et al., 2022), which usually records the maximum temperature of the sedimentary basin and the highest maturity level that source rocks have reached (Mukhopadhyay, 1994). In contrast to stratigraphic maturity, the thermal maturity of reservoired petroleum is distinct due to a time-dependent process of petroleum expulsion, migration and secondary alterations. Oil expulsion from source rocks typically occurs continuously over millions of years (Huang et al., 2022). In basins with multiple charging periods, reservoired petroleum often represents a mixture of compounds with a broad range of stratigraphic maturity, rather than the final trapped fractions. As a result, it is challenging to assess the thermal maturity of reservoired petroleum using a single maturity value, as is done for the stratigraphic maturity of source rocks. Under such circumstances, the concept of "mass fraction maturity" was introduced which reflects the cumulative relationship on fractional masses of petroleum generated and expelled from source rocks of varied stratigraphic maturity over geological times, incorporating the effects of charging histories (Wilhelms and Larter, 2004; Huang et al., 2022).

An instantaneous petroleum charge was initially regarded as the petroleum in the source rock, which is effectively at a maturity level equivalent to the stratigraphic maturity of the source rock. In most cases, reservoired oils represent continuous and cumulative petroleum wherein each molecular component exhibits a distinct concentration profile corresponding to the stratigraphic maturity of source rocks (Huang et al., 2022). Biomarkers, such as terpanoids and steroids, are abundant in immature and marginally mature oils but decline sharply during the early oil generation stage, eventually becoming undetectable at high maturity levels (Wilhelms and Larter, 2004). Consequently, maturity estimated by biomarkers is the minimum maturity at the time of expulsion. In contrast, aromatic hydrocarbons, which are more likely retained in the source rocks during petroleum expulsion, are indicative of maximum maturity levels (Huang et al., 2022). However, reservoired petroleum could be considered as an instantaneous petroleum charge when oil expelled from a source rock over a very narrow maturity range, an uncommon phenomenon in sedimentary basins. In this study, an end member of instantaneous petroleum charge is proposed in the Tarim Basin, to provide insights into the geochemical property of individual petroleum charge as well as hydrocarbon accumulation of ultra-deep Ordovician reservoirs.

2 Geological settings

The Tarim Basin is a typical petroliferous basin with multiple charge stages and complex mixing scenarios in northwest China. Since Phanerozoic, the basin has experienced significant tectonic activities. Regional extension occurred in the Tarim Basin from the Early Paleozoic to the Middle Ordovician (Jia, 1997). Large-scale central paleo-uplift and the northern depression were developed at the end of the Middle Ordovician, including the Shuntuoguole low uplift, the Awati depression, and the Manjiaer depression (Qiu et al., 2019). From the Middle to Late Ordovician, the strata witnessed erosion due to uplift in the Tazhong area, whereas it was a platform-slope in the Tabei area (Deng et al., 2022). The Tabei area uplifted and eroded at the end of Ordovician and the Middle Devonian. During the Permian, Tazhong uplift remained relatively stable whereas the Tabei uplift suffered intensive uplift and erosion. Therefore, early-charged petroleum witnessed various secondary alterations and multi-charging periods, resulting in complicated geochemical profiles of reservoired oils (Zhu et al., 2012; Zhang et al., 2014). It remains challenging to figure out an end member of instantaneous petroleum charge that can be correlated to a specific stratigraphic maturity to unravel the geochemical signatures of individual charging episode.

The Shunbei area, crucial ultra-deep petroleum reservoirs in the Tarim Basin, located in the Shuntuoguole low uplift which is surrounded by the Tabei uplift, the Tazhong uplift, the Awati depression, and the Manjiaer depression (Figure 1a). Numerous research has been conducted on liquid petroleum accumulation and preservation within reservoirs of depth below 8,000 m. Currently, petroleum in the Shunbei reservoirs is primarily generated from individual source rocks discontinuously in the Cambrian Yuertusi Formation (Zhang and Huang, 2005; Zhang et al., 2005, 2011) during the Caledonian, Hercynian, Yanshanian and/or Himalayan periods (Wu et al., 2023; Yang et al., 2024). Petroleum has accumulated in the Ordovician Yingshan ($O_{1\text{-}2}y$) and Yijianfang (O_2yj) formations where limestone predominates in the sediments. Starting from the latest Middle Ordovician, strike-slip faults of multiphase activities formed as reservoir-scale fault damage zones in the Lower–Middle Ordovician carbonates and cut through the Lower Cambrian source rocks. Muti-phase activities of strike-slip faults in reservoir-scale fault damage zones are well developed in the Shunbei area (Qiu et al., 2019; Wu et al., 2019; Jiang et al., 2024), which play a critical role in facilitating petroleum migration and accumulation (Deng et al., 2022; Liu et al., 2023, 2024). The thick mudstones performed as cap rock in the Upper Ordovician (Figure 1c).

3 Samples and methods

3.1 Samples

An oil sample from Well Shunbei 3 (SHB3), located in the No.3 fault zone in the Shunbei area, was collected in the Ordovician Yingshan Formation at a depth of 7,518.8–7,891.3 m (Figure 1b). In comparison, ten Ordovician oil samples were collected from the No.1 fault zone in Shunbei reservoirs at a depth of 7,229.5–8,225.4 m

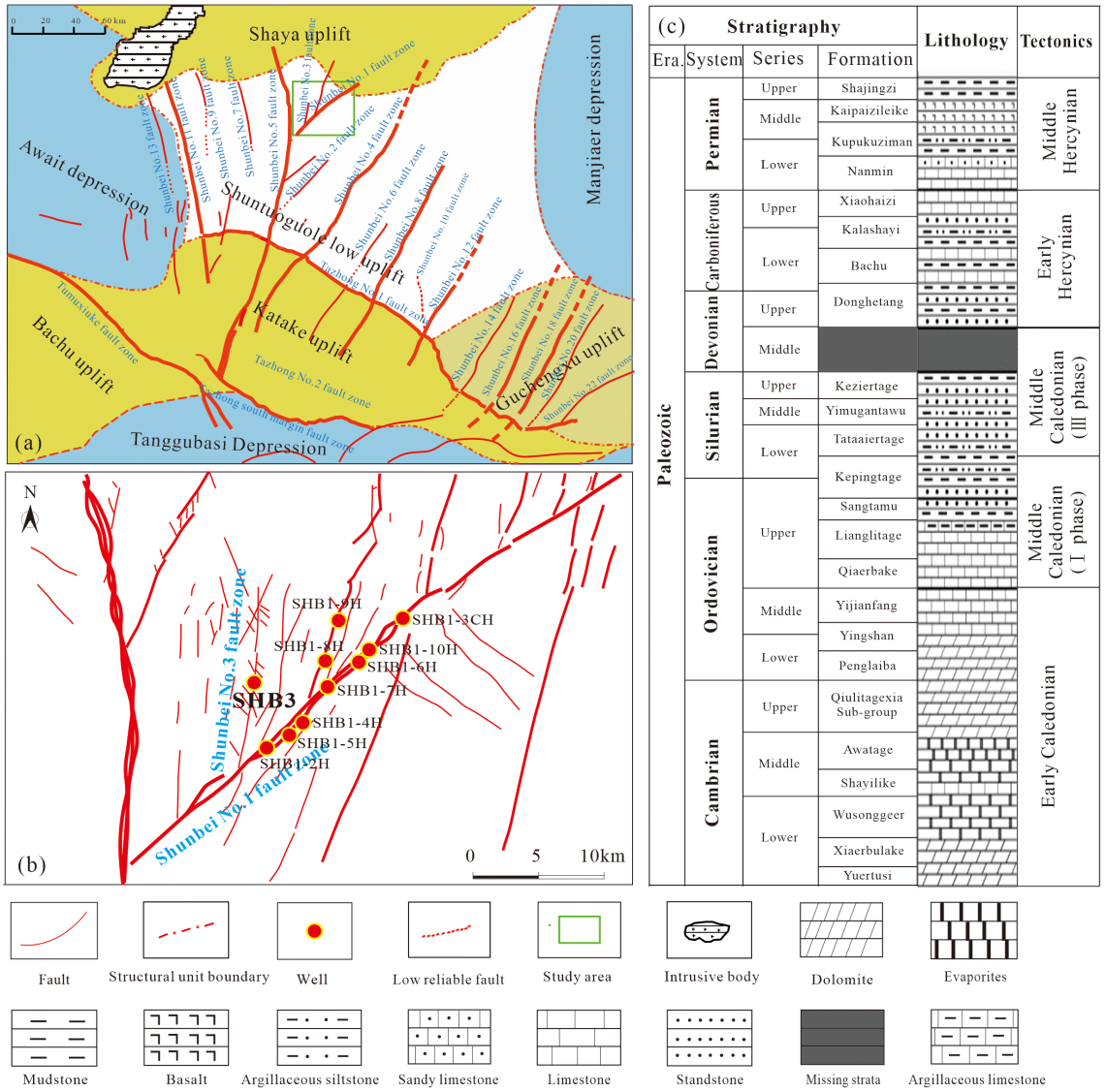

FIGURE 1
Geological settings. **(a)** Strike-slip faults in the northern Tarim Basin (modified after Liu, 2020). **(b)** Sample locations. **(c)** The general Paleozoic stratigraphy of the Shunbei area, Tarim Basin (modified after Deng et al., 2022).

(Figure 1b). These samples are typical volatile oils from ultra-deep carbonate reservoirs in the Shunbei area. The oils exhibit high API gravity ranging from 42.27° to 47.84° (Table 1). To avoid light hydrocarbon volatilization, all the samples were sealed in amber airtight vials and stored under refrigeration prior to experimentation.

3.2 Gas chromatography-mass spectrometry analysis

Petroleum composition analysis was conducted in the PRG lab, University of Calgary. First, asphaltenes were removed from the oil samples on a polar Florisil solid phase extraction (SPE) cartridge by hexane and dichloromethane to obtain total hydrocarbon. The total hydrocarbon was then fractionated into the saturated and aromatic hydrocarbon fractions by solvents including pentane, dichloromethane and isopropyl alcohol in a custom-made silica gel column. A suite of internal standards including squalane, cholestane-d_4, adamantane-d_{16}, naphthalene-d_8, phenanthrene-d_{10} and 1,1′-binaphthyl, was added in the oil samples to enable quantification of petroleum compositions. Finally, the saturated and aromatic hydrocarbons were performed on an Agilent 7890B gas chromatograph linked to an Agilent 5977A MSD system. Instrument settings and operating procedures followed those described by Wang et al. (2021a).

4 Results

4.1 *n*-Alkanes and isoprenoids

The oils from both the No.1 and No.3 fault zones contain abundant *n*-alkanes and isoprenoids (Figure 2). Although

TABLE 1 Oil sample physical property and related parameters derived from saturated hydrocarbons.

Well	Depth (m)	Strata	API°	n-C_{20-}/n-C_{21+}	Pr/n-C_{17}	Ph/n-C_{18}	Pr/Ph	C_{29} 20S/(20S+20R)	C_{29} ββ/(αα+ββ)	Ts/(Ts+Tm)	C_{23}TT/C_{30}H
SHB1-2H	7469.0–7569.5	O_2yj	46.26	3.00	0.29	0.42	0.79	0.47	0.51	0.76	3.30
SHB1-3CH	7255.7–7357.9	O_2yj	46.71	2.77	0.32	0.45	0.80	0.50	0.48	0.87	15.79
SHB1-4H	7459.0–7562.0	O_2yj	46.49	2.96	0.32	0.44	0.78	0.42	0.46	0.84	6.73
SHB1-5H	7474.5–7576.2	O_2yj	45.82	2.83	0.33	0.48	0.79	0.45	0.53	0.87	5.04
SHB1-6H	7288.2–7399.8	O_2yj	47.84	2.26	0.32	0.44	0.79	0.48	0.48	0.68	8.56
SHB1-7H	7339.4–7456.0	O_2yj	45.60	2.70	0.31	0.45	0.78	0.45	0.54	0.69	5.63
SHB1-8H	7415.5–7571.6	$O_{1-2}y$	45.82	2.35	0.31	0.44	0.77	0.44	0.46	0.90	12.32
SHB1-9	7372.7–7630.0	$O_{1-2}y$	44.50	2.30	0.32	0.47	0.76	0.43	0.46	0.92	11.74
SHB1-10H	7229.5–8225.4	$O_{1-2}y$	44.50	2.25	0.32	0.46	0.78	0.47	0.45	0.55	2.11
SHB3	7518.8-7891.3	$O_{1-2}y$	42.27	1.50	0.12	0.15	0.83	N/A	N/A	N/A	N/A

A part of alkane-related data was collected from Wang et al., 2025.

biodegradation is common in the Tarim Basin, particularly in Silurian reservoirs in the Tazhong area (Wang et al., 2020), the analyzed samples from the Shunbei area appear to show no signs of biodegradation.

However, noteworthy difference occurred to *n*-alkane and isoprenoid distribution patterns between oil samples from the No.1 and No.3 fault zones (Figure 2). Oil samples from the No.1 fault zone, exhibit similar *n*-alkane and isoprenoid distribution patterns, with low carbon *n*-alkanes dominating over relatively higher carbon *n*-alkanes (Figure 3). The n-C_{20-}/n-C_{21+} ratios of oil samples from the No.1 fault zone range from 2.25 to 3.00 (Table 1). The isoprenoids, pristane and phytane, are in obvious lower concentrations compared to the adjacent *n*-alkanes, with Ph/n-C_{18} and Pr/n-C_{17} ratios in the ranges of 0.42–0.48, and 0.29–0.33, respectively (Table 1). In contrast, SHB3 oil has a noteworthy predominance of high-carbon-number *n*-alkanes (> C_{19}) but less abundant light *n*-alkanes (< C_{16}) (Figure 3) with a relatively lower n-C_{20-}/n-C_{21+} ratio (Table 1). Additionally, SHB3 oil is characterized by low concentrations of pristane and phytane, with low Ph/n-C_{18} and Pr/n-C_{17} ratios below 0.15 (Table 1).

4.2 Steroids and terpenoids

Steroids and terpenoids are common biomarkers in crude oils with compound identification and abbreviation shown in Table 2. However, significant discrepancy occurs in steroid and terpenoid distribution patterns between oils from the No.1 and No.3 fault zones. In the oil samples from the No.1 fault zone, steroids are present but generally in low concentrations (Figure 4a), typically below 10 ppm, with C_{21} pregnane being relatively higher in a range of 13–17 ppm. The concentrations of regular and rearranged steranes show little variation among these oil samples (Figure 5a). Maturity parameters derived from steroids including C_{29} 20S/(20S + 20R) and C_{29} ββ/(αα + ββ) fall in narrow ranges, i.e., 0.42–0.50 and 0.45–0.54 (Table 1), respectively, implying similar maturity levels of these oil samples. In contrast, SHB3 oil is absent from steroids (Figure 5a).

Similar to the distribution patterns of steroids, terpenoids including tricyclic terpanes (TTs), tetracyclic terpane (TeT) and pentacyclic terpanes (PTs), have been identified in oil samples from the No.1 fault zone (Figure 4b) with C_{19}–C_{25} TTs being the most abundant ranging from 20 to 30 ppm in concentration. The Ts/(Ts + Tm) ratio, a maturity parameter derived from terpenoids, varies between 0.55 to 0.92 in these samples (Table 1). However, the C_{23}TT/C_{30}H values exhibit greater variability (Table 1), primarily due to trace amount of C_{30}H in this formula. As a result, caution should be taken when interpreting these ratios due to low concentrations of individual components. In contrast, similar to steroids in SHB3 oil, no individual terpenoid components are detected in these samples (Figure 5b).

4.3 Diamondoid hydrocarbons

Adamantane, diamantane and their homologs are detected in all the oil samples (Figures 6, 7). Generally, SHB3 oil exhibits lower concentrations of diamondoid hydrocarbons compared to samples from the No.1 fault zone (Figure 8). For both sets of oil samples, diamantane species have lower concentrations than their *methyl-*, *dimethyl-* and *trimethyl*-substituted isomers, with a notable decrease in tetramethyldiamantane concentrations (Figure 8). Among the oil samples from the No.1 fault zone, the 1,3-dimethyladamantane (1,3-DMAD) and 1-methyladamantane (1-MAD) are the most abundant species, with concentrations ranging from 192–291 and 314–327 ppm, respectively. Both adamantane and diamantane in the No.1 fault zone samples show similar aggregated concentrations of approximately 50–70 ppm. Maturity-related parameters such as the methyladamantane index [MAI=1-MAD/(1-MAD+2-MAD)] and methyldiamantane index [MDI=4-MD/(1-MD+3-MD+4-MD)] exhibit minor variation,

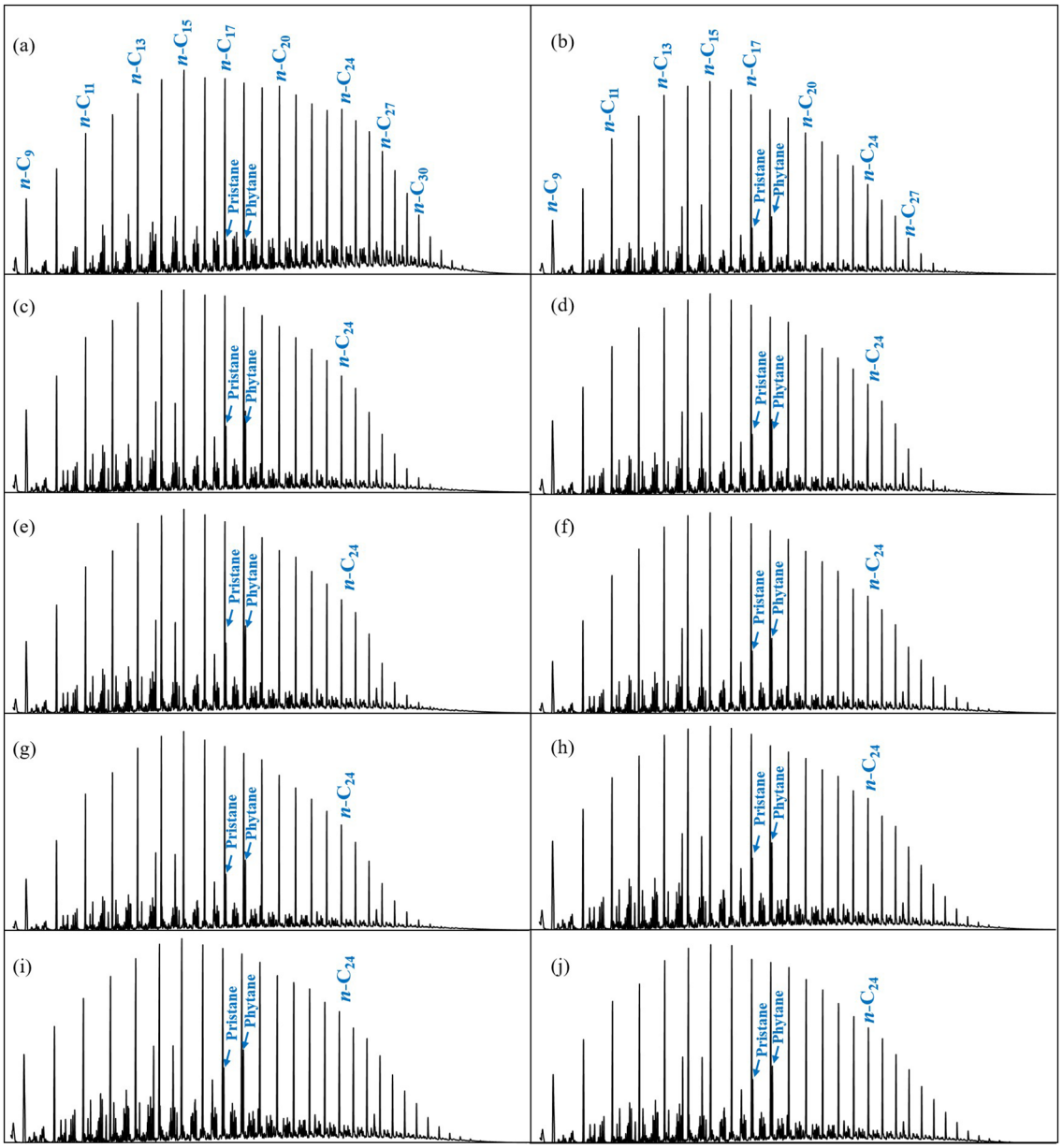

FIGURE 2
Mass chromatograms of *m/z* 85 showing occurrences of *n*-alkanes and isoprenoids. **(a)** SHB3 oil, O_2yj. **(b)** SHB1-2H oil, O_2yj. **(c)** SHB1-3CH oil, O_2yj. **(d)** SHB1-4H oil, O_2yj. **(e)** SHB1-5H oil, O_2yj. **(f)** SHB1-6H oil, O_2yj. **(g)** SHB1-7H oil, O_2yj. **(h)** SHB1-8H oil, $O_{1\text{-}2}y$. **(i)** SHB1-9 oil, $O_{1\text{-}2}y$. **(g)** SHB1-10 oil, $O_{1\text{-}2}y$.

ranging from 2.31–2.69 and 0.43–0.46, respectively, for the No.1 fault zone (Table 3). In contrast, SHB3 oil has significantly lower concentrations of diamondoid hydrocarbons, with individual components generally below 100 ppm. The concentration differences of adamantane and diamantane species are less pronounced in SHB3 oil compared to those from the No.1 fault zone. Methylated diamantanes (15–49 ppm) are notably less abundant than methylated adamantanes in SHB3 oil. SHB3 oil also shows a lower MAI value (MAI=1.65) but a slightly higher MDI value (MDI=0.52) compared to the No.1 fault zone oils (Table 3).

4.4 Aromatic hydrocarbons

The aromatic molecular parameters are more reliable indicators of thermal maturity at relatively high maturity levels. Consistent with this, monoaromatic and triaromatic steroids are absent in all the analyzed oil samples, further supporting their high maturity. Among the aromatic hydrocarbon series, alkylnaphthalenes are the most abundant. The 2-methylnaphthalene (2-MN) exhibits the highest concentration, exceeding 800 ppm, followed by 26,27-dimethylnaphthalene (26,27-DMN), which ranges from 694 to 819 ppm. Among all the studied oils, 2-MN has a pronounced dominance

10.3389/fmars.2025.1553799

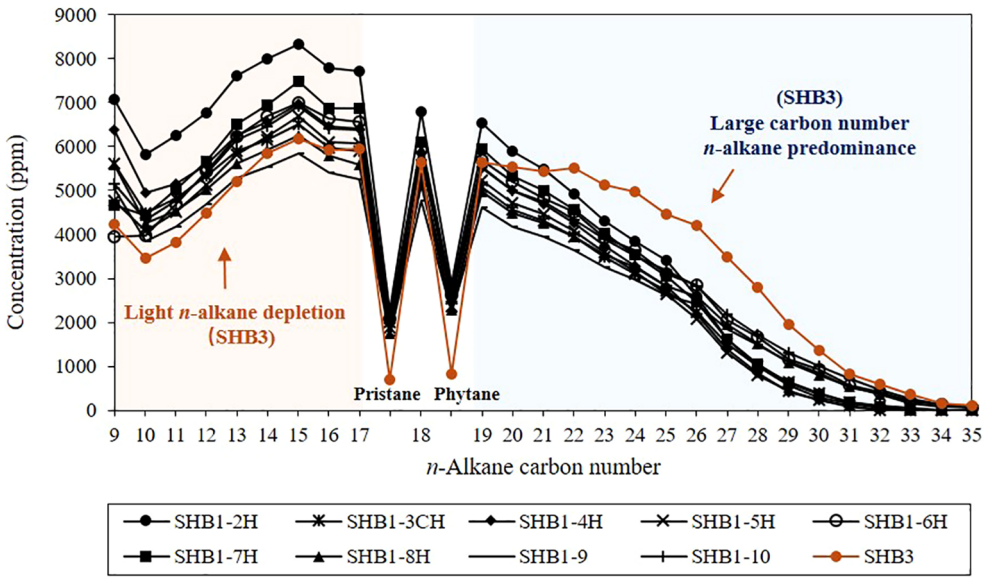

FIGURE 3
n-Alkane and isoprenoid concentration and distribution of oil samples from the No.1 and No.3 fault zones.

TABLE 2 Steroids and terpenoids in this study.

No.	Compound	Abbreviation	No.	Compound	Abbreviation
1	C_{21} pregnane	21PREG	30	C_{22} tricyclic terpane	22TT
2	C_{22} pregnane	22PREG	31	C_{23} tricyclic terpane	23TT
3	C_{27} 10β(H),13α(H) 20S diasterane	27βαS	32	C_{24} tricyclic terpane	24TT
4	C_{27} 10β(H),13α(H) 20R diasterane	27βαR	33	C_{25} tricyclic terpane	25TT
5	C_{27} 10α(H),13β(H) 20S diasterane	27αβS	34	C_{24} tetracyclic terpane	24TeT
6	C_{27} 10α(H),13β(H) 20R diasterane	27αβR	35	C_{26} tricyclic terpane	26TT
7	C_{28} 10β(H),13α(H) 20S diasterane	28βαS	36	C_{28} tricyclic terpane	28TT
8	C_{28} 10β(H),13α(H) 20R diasterane	28βαR	37	C_{29} tricyclic terpane	29TT
9	C_{28} 10α(H),13β(H) 20S diasterane	28αβS	38	18α(H)-22,29,30-trisnorneohopane	Ts
10	C_{28} 10α(H),13β(H) 20R diasterane	28αβR	39	17α(H)-22,29,30-trisnorhopane	Tm
11	C_{29} 10β(H), 13α(H) 20S diasterane	29βαS	40	C_{30} tricyclic terpane	30TT
12	C_{29} 10β(H),13α(H) 20R diasterane	29βαR	41	C_{28} bisnorneohopane	28BH
13	C_{29} 10α(H),13β(H) 20S diasterane	29αβS	42	C_{29} 17α(H),21β(H) hopane	29H
14	C_{29} 10α(H),13β(H) 20R diasterane	29αβR	43	18-α(H)-30-norneohopane	29Ts
15	C_{27} 5α(H),14α(H),17α(H) 20S sterane	27ααααS	44	C_{30} diahopane	30DiaH
16	C_{27} 5α(H),14α(H),17α(H) 20R sterane	27αααR	45	C_{29} 17β(H),21α(H) hopane	29M
17	C_{27} 5α(H),14β(H),17β(H) 20R sterane	27αββR	46	C_{30} 17α(H),21β(H) hopane	30H
18	C_{27} 5α(H),14β(H),17β(H) 20S sterane	27αββS	47	C_{30} 17β(H),21α(H) hopane	30M
19	C_{28} 5α(H),14α(H),17α(H) 20S sterane	28ααααS	48	C_{31} 17α(H),21β(H) 22S homohopane	31HS
20	C_{28} 5α(H),14β(H),17β(H) 20R sterane	28αββR	49	C_{31} 17α(H),21β(H) 22R homohopane	31HR

(Continued)

TABLE 2 Continued

No.	Compound	Abbreviation	No.	Compound	Abbreviation
21	C_{28} 5α(H),14β(H),17β(H) 20S sterane	28αββS	50	gammacerane	GAM
22	C_{28} 5α(H),14α(H),17α(H) 20R sterane	28αααR	51	C_{32} 17α(H),21β(H) 22S homohopane	32HS
23	C_{29} 5α(H),14α(H),17α(H) 20S sterane	29αααS	52	C_{32} 17α(H),21β(H) 22R homohopane	32HR
24	C_{29} 5α(H),14β(H),17β(H) 20R sterane	29αββR	53	C_{33} 17α(H),21β(H) 22S homohopane	33HS
25	C_{29} 5α(H),14β(H),17β(H) 20S sterane	29αββS	54	C_{33} 17α(H),21β(H) 22R homohopane	33HR
26	C_{29} 5α(H),14α(H),17α(H) 20R sterane	29αααR	55	C_{34} 17α(H),21β(H) 22S homohopane	34HS
27	C_{19} tricyclic terpane	19TT	56	C_{34} 17α(H),21β(H) 22R homohopane	34HR
28	C_{20} tricyclic terpane	20TT	57	C_{35} 17α(H),21β(H) 22S homohopane	35HR
29	C_{21} tricyclic terpane	21TT	58	C_{35} 17α(H),21β(H) 22R homohopane	35HS

over 1-MN, indicating a higher maturity level. Methylated naphthalenes are detectable up to tetramethylnaphthalenes (TeMNs), while pentamethylnaphthalenes (PMNs) are only in trace amount or even absent in oil samples from the No.1 fault zone. Notably, SHB3 oil shows a relatively higher proportion of TMNs, TeMNs and PMNs (Table 4). Several maturity parameters derived from alkylnaphthalene have been established, including MNR (= 2-MN/1-MN) (Radke et al., 1982a), DNR [= (2,6-DMN + 2,7-DMN)/1,5-DMN] (Radke et al., 1986), TMNr [= 1,3,7-TMN/(1,3,7-TMN + 1,2,5-TMN] (van Aarssen et al., 1999), TeMNr [= 1,3,6,7-TeMN/(1,3,6,7-TeMN + 1,2,5,6-TeMN + 1,2,3,5-TeMN)]) (van Aarssen et al., 1999), and PMNr [= 1,2,4,6,7-PMN/(1,2,4,6,7-PMN + 1,2,3,5,6-PMN)] (van Aarssen et al., 1999). However, parameters such as TeMNr and PMNr, become invalid in highly mature

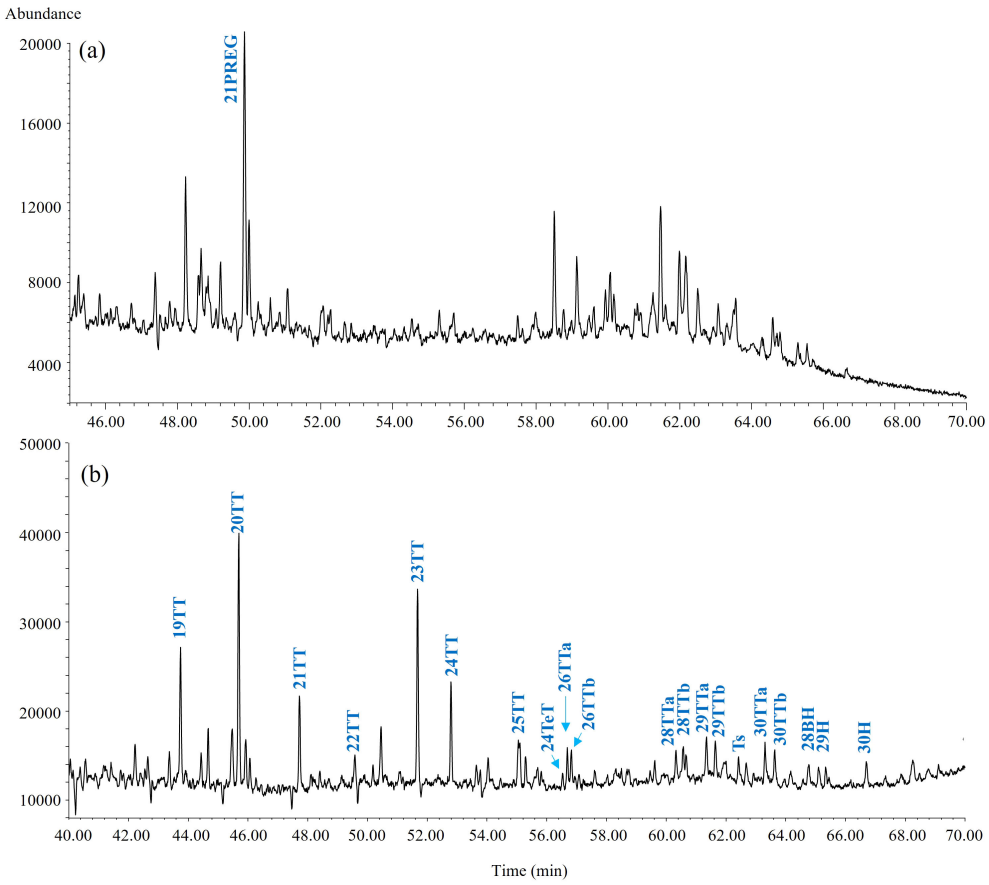

FIGURE 4
Partial mass chromatograms of *m/z* 217 and 191 showing typical distribution of steroids and terpenoids of SHB1-7H oil, respectively. **(a)** Steroids. **(b)** Terpenoids. PREG, pregnane; TT, tricyclic terpanes; TeT, tetracyclic terpane; PT, pentacyclic terpane; BH, bisnorneohopane; H, hopane.

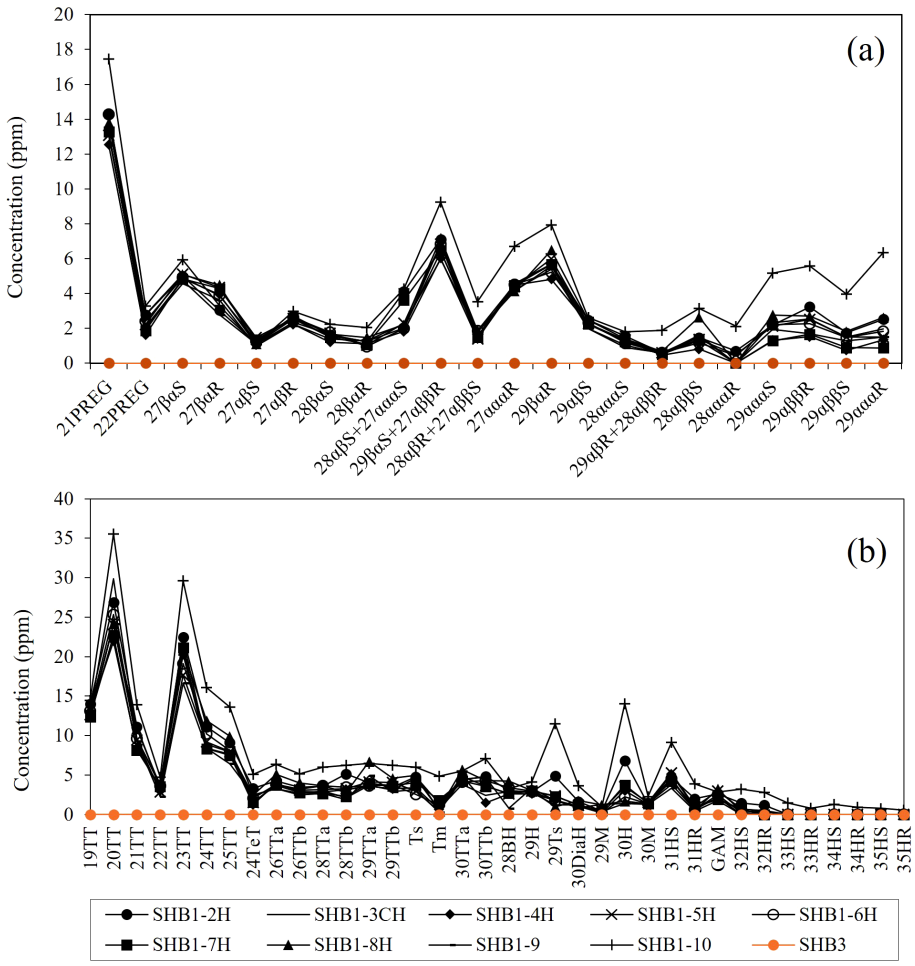

FIGURE 5
Steroid and terpenoid distribution patterns of oil samples from the No.1 and No.3 fault zones. **(a)** Steroids. **(b)** Terpenoids.

petroleum or sediments with vitrinite reflectance above 1.1% while those derived from *methyl-* or *dimethyl-* substituted naphthalenes remain valid (Wang et al., 2022). Consequently, MNR, DNR and TMNr are accepted for assessing thermal maturity in this study. The MNR and DNR values of oil samples from the No.1 fault zone range from 1.95–2.17 and 9.23–11.33, respectively, whereas those of SHB3 oil are relatively lower (Table 3). As the proportion of TMNs increases in SHB3 oil, the discrepancy in TMNr values of oils from the No.1 and No.3 fault zones diminishes.

Dibenzothiophene (DBT) and methyldibenzothiophenes (MDBTs) are also significant components of aromatic hydrocarbons in oil samples from the No.1 fault zone (Figure 9). Concentrations of DBT, 4-MDBT and 2-+3-MDBT exceed 100 ppm, whereas the less stable isomer, 1-MDBT, is below 10 ppm. A stark contrast is observed in SHB3 oil, where concentrations of DBT and MDBTs are below 5 ppm (Figure 9). The methyldibenzothiophene index (MDR = 4-MDBT/1-MDBT) (Radke et al., 1986) ranges from 20.95 to 26.48 for oil samples from the No.1 fault zone, while SHB3 oil shows a slightly lower MDR of 20.67 (Table 3). Phenanthrene (P) concentrations in oil samples from the No.1 fault zone are approximately 100 ppm, compared to 64 ppm in SHB3 oil. Based on previous research, the MPI-3 parameter [= (3-MP + 2-MP)/(9-MP + 1-MP)] has proven to be a reliable indicator at highly maturity levels (He et al., 2019), whereas MPI-1 [= 1.5 × (2-MP + 3-MP)/(P + 1-MP + 9-MP)] (Radke et al., 1982b) and MPI-2 [= 3 × 2-MP/(P + 1-MP + 9-MP)] (Radke et al., 1982b) show poor correlation with thermal maturity due to the faster increase of phenanthrene, which compensates for the thermal stability impact on methylphenanthrene isomers. The MPI-3 values for all studied oils are similar, ranging from 1.04 to 1.24 (Table 3). Maturity parameters derived from biphenyl (BP) are more sensitive to thermal maturation (Alexander et al., 1986; Cumbers and Alexander, 1987; Wang et al., 2019). The methylbiphenyl (MBP) index (MBPI = 4-MBP/2-MBP), is valid in a wide maturity range of 0.4–1.6%Ro (Wang et al., 2019). The MBPI values of oil samples from the No.1 fault zone range from 60.34 to 110.99, whereas SHB3 oil is merely 3.75 (Table 3). The calculated vitrinite reflectance (%Rc) obtained from MBPI, was proposed by Wang et al. (2019), i.e., %Rc= 7.49 × 10^{-3} MBPI + 0.794 (%R>0.8). The %Rc of oil samples from the No.1 fault zone

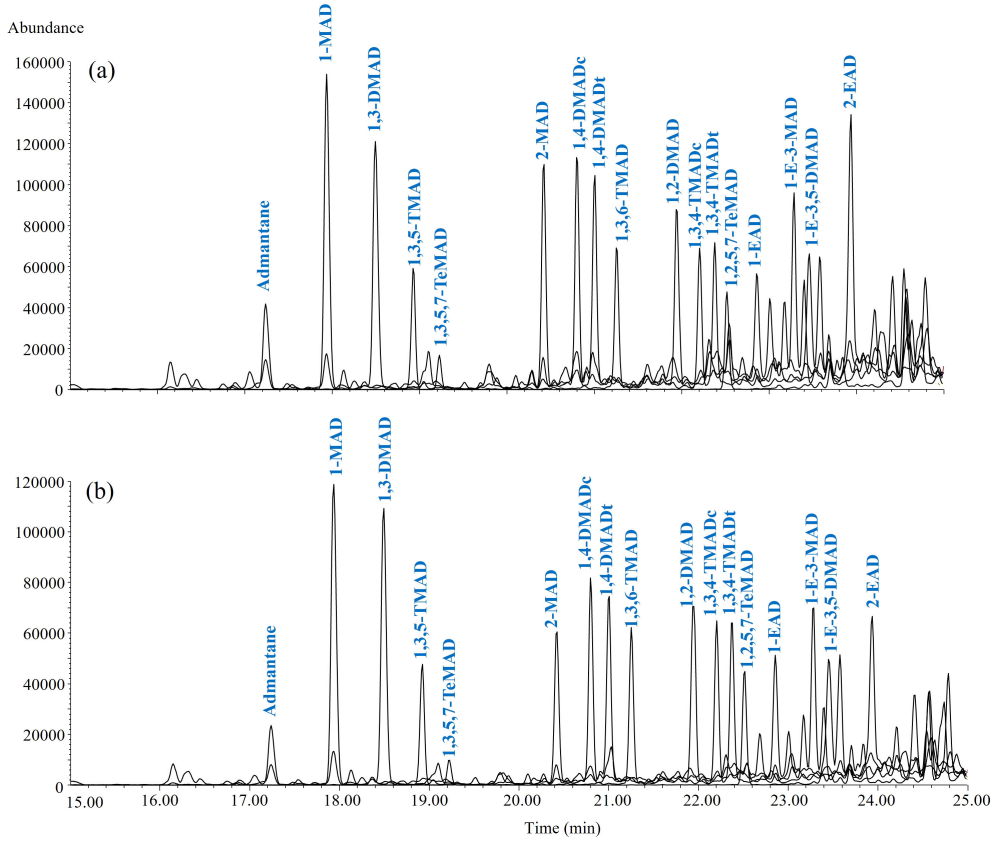

FIGURE 6
Summed mass chromatograms of *m/z* 136, 135, 149, 163, and 177 showing typical distribution of alkylated admantanes. **(a)** SHB3 oil. **(b)** SHB1-7H oil. MAD, methyladmantane; DMAD, dimethyladmantane; TMAD, trimethyladmantane; TeMAD, tetramethyladmantane; EAD, ethyladmantane.

range from 1.25 to 1.63, whereas SHB3 oil is much lower in maturity with %Rc at 0.82 (Table 3).

5 Discussion

5.1 SHB3 oil as an end member of instantaneous petroleum charge

Thermal maturity exerts significant impact on component concentrations of reservoired petroleum. Regular steranes with biological configuration (e.g., C_{27}-C_{29} ααα*R*) dominate immature petroleum fractions, whereas steranes with geological configurations (e.g., αααS, αββR and αββS) along with pregnanes and diasteranes, are less abundant in immature petroleum. However, as thermal maturity increases, the relative abundance of steranes with geologically configurations, as well as pregnanes and diasteranes, increase dramatically. The thermal maturity parameter C_{29} 20S/(20S + 20R) was introduced to measure the isomerization of C_{29} steranes at the C-20 chiral center and the transformation of biological αα and ββ epimers during thermal evolution (Seifert and Moldowan, 1978). Generally, sterane isomerization between biological and geological configurations reaches equilibrium at approximately 0.8%Ro, with a maximum C_{29} 20S/(20S + 20R) value of around 0.65. Notably, steranes become undetectable beyond a maturity threshold of approximately 1.1%Ro, as no steranes are observed at higher levels of thermal maturity.

Oil mixing is a common phenomenon in the Tarim Basin, where the proportions and maturity of the end members dominate the maturity parameters derived from biomarkers. As noted by Huang et al. (2022), the C_{29} 20S/(20S + 20R) ratio is 0.18 when 5% by mass of the very low maturity (Ro=0.5%) that is rich in biomarkers are mixed with 95% of a late generated mature oil (Ro=1.0%). In this scenario, the C_{29} 20S/(20S + 20R) ratio shows a "mature" signature only if the proportion of low maturity oil decreases to less than 1%. If the biomarker concentrations of one end member (Ro=0.65%) decrease while the other end member remains at 1.0%Ro, the C_{29} 20S/(20S + 20R) ratio increases to 0.44 and 0.52 when 50% and 5% by mass of the end member oil at 0.65%Ro is included, respectively. The C_{29} 20S/(20S + 20R) ratios in the oil samples from the No.1 fault zone range from 0.42 to 0.50, indicating contributions from early-charged oil. However, these ratios also reflect dilution caused by subsequent generations of petroleum at higher maturity levels, during which regular steranes and diasteranes were destroyed. In contrast, the absence of steranes in SHB3 oil suggests it did not receive the early-charged oil.

As highlighted in the component concentration profiles by Huang et al. (2022), isoprenoid alkanes constitute a significant proportion of petroleum at low maturity stages (Ro<0.6%) compared to *n*-alkanes.

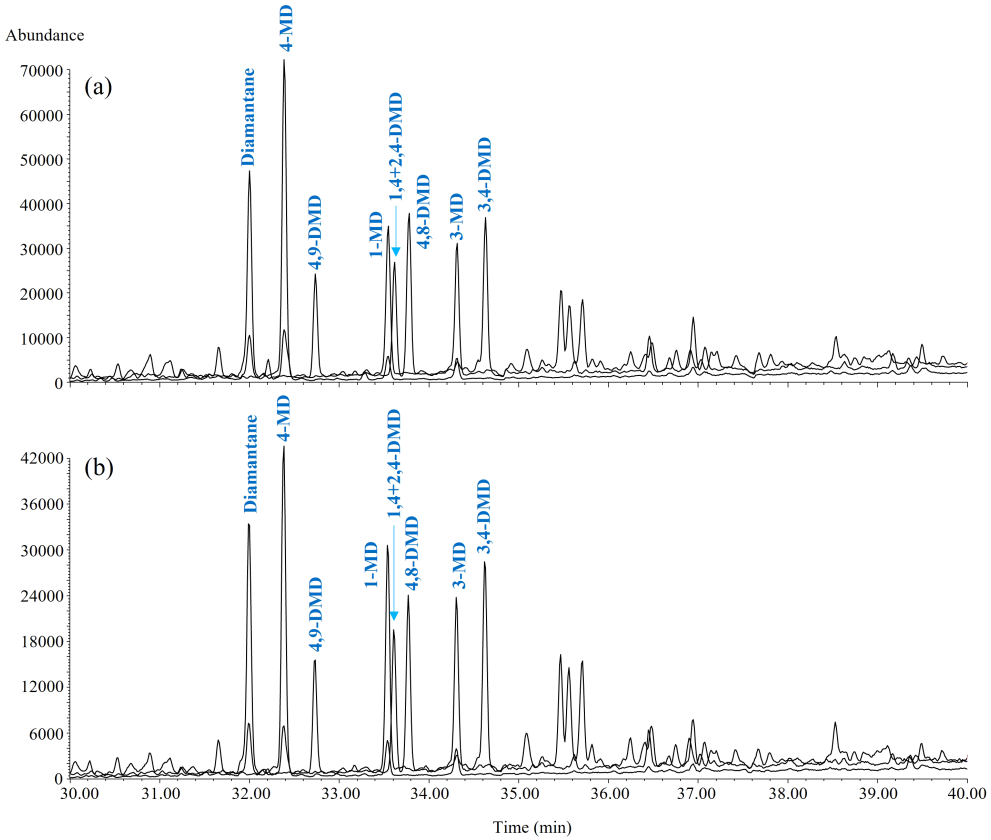

FIGURE 7
Summed mass chromatograms of *m/z* 188, 187, and 201 showing typical distribution of alkylated diamantanes. **(a)** SHB3 oil. **(b)** SHB1-7H oil. MD, methyladamantane; DMD, dimethyladamantane.

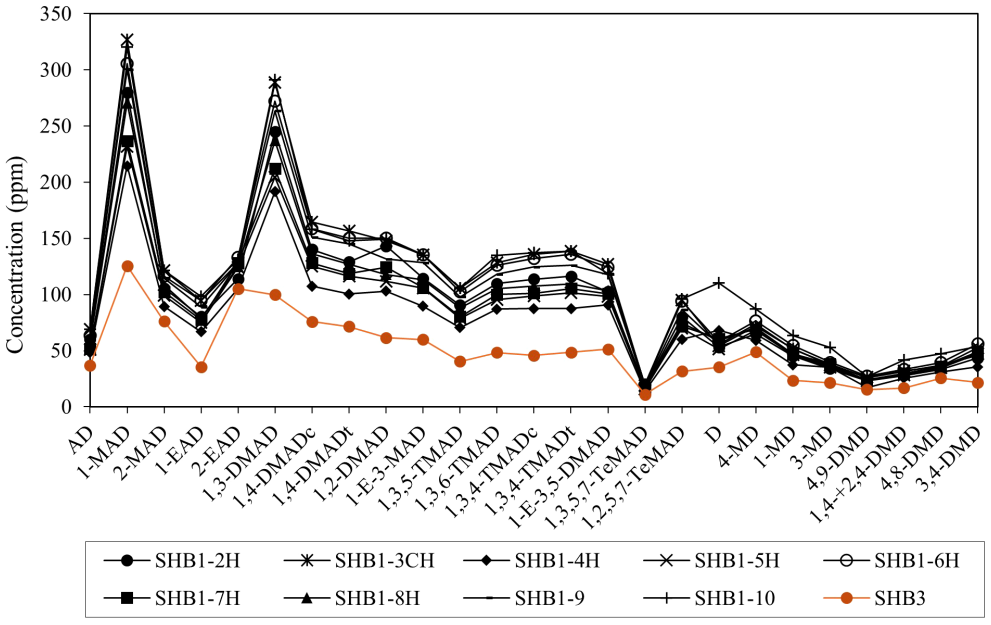

FIGURE 8
Concentrations of alkylated admantanes and diamantanes.

10.3389/fmars.2025.1553799

TABLE 3 Thermal maturity parameters.

Well	Depth (m)	Strata	MAI	MDI	MNR	DNR	TMNr	MPI-3	MBPI	%Rc
SHB1-2H	7469.0–7569.5	O_2yj	2.65	0.45	2.12	10.43	0.89	1.17	93.25	1.49
SHB1-3CH	7255.7–7357.9	O_2yj	2.69	0.45	2.16	10.62	0.90	1.24	94.06	1.50
SHB1-4H	7459.0–7562.0	O_2yj	2.40	0.45	2.15	11.33	0.92	1.16	77.64	1.38
SHB1-5H	7474.5–7576.2	O_2yj	2.33	0.45	2.11	11.13	0.91	1.16	78.86	1.38
SHB1-6H	7288.2–7399.8	O_2yj	2.63	0.45	2.17	10.88	0.90	1.23	104.84	1.58
SHB1-7H	7339.4–7456.0	O_2yj	2.31	0.45	2.13	11.17	0.91	1.17	86.15	1.44
SHB1-8H	7415.5–7571.6	$O_{1\text{-}2}y$	2.50	0.46	1.95	9.23	0.90	1.04	60.34	1.25
SHB1-9	7372.7–7630.0	$O_{1\text{-}2}y$	2.62	0.45	2.01	9.63	0.89	1.12	82.48	1.41
SHB1-10H	7229.5–8225.4	$O_{1\text{-}2}y$	2.63	0.43	2.10	10.42	0.88	1.18	110.99	1.63
SHB3	7518.8-7891.3	$O_{1\text{-}2}y$	1.65	0.52	1.94	8.85	0.91	1.09	3.75	0.82

However, the relative abundance of pristane and phytane decreases dramatically against the adjacent *n*-alkanes, i.e., Pr/*n*-C_{17} and Ph/*n*-C_{18}, as maturity increases. The Pr/*n*-C_{17} and Ph/*n*-C_{18} values of SHB3 oil are notably lower than those from the No.1 fault zone, indicating that the reservoir associated with Well SHB3 lacks the early petroleum charging. In contrast, the reservoir within the No.1 fault zone underwent multiple episodes of petroleum charging, with early-charged petroleum characterized by high Pr/*n*-C_{17} and Ph/*n*-C_{18} values. Although subsequent petroleum charges at the higher maturity levels were accumulated in the reservoir with lower Pr/*n*-C_{17} and Ph/*n*-C_{18} values, it did not significantly alter the relatively high Pr/*n*-C_{17} and Ph/*n*-C_{18} values established by the early-charged petroleum.

While the biomarkers such as streranes and terpanes are most abundant in low-maturity petroleum fractions, aromatic hydrocarbons become predominate during later stages of petroleum generation (Wilhelms and Larter, 2004). Aromatic compounds with C–S bonds cyclized in fused aromatic structures, such as DBTs, are typically more thermally stable than those with C–C bonds, e.g., MNs (Wang et al., 2021b). The SHB3 oil exhibits lower concentrations of DBT and MDBTs compared to oils from the No.1 fault zone (Figure 9), indicating that the maturity of later-charged petroleum in SHB3 oil is lower than that in the No.1 fault zone. This is further supported by the lower values of parameters derived from MNs, DMNs and MDBTs, such as MNR, DNR and MDR, in SHB3 oil compared to those from the No.1 fault zone. Another compelling piece of evidence lies in the higher relative proportion on TMNs, TeMNs and PMNs of SHB3 oil. These compounds are preserved because the high degree of alkyl substitution in SHB3 oil has not been thermally cracked, unlike in the more mature oils from the No.1 fault zone.

Additionally, diamondoid hydrocarbons, which are sensitive indicators to multiple hydrocarbon charges and typically generated during later maturation stages (Zhang et al., 2005), are more abundant in oil samples from the No.1 fault zone than in SHB3 oil (Figure 8). This suggests that the reservoir associated with Well SHB3 has not undergone petroleum charging during the very late maturation stages. SHB3 oil spans a very narrow maturity range, which can be regraded as instantaneous petroleum charge (Figure 10). This is evident from the absence of the earliest charged

TABLE 4 Normalized content of methylated naphthalenes.

Well	Depth (m)	N (%)	MNs (%)	DMNs (%)	TMNs (%)	TeMNs (%)	PMNs (%)
SHB1-2H	7469.00–7569.47	6.38	26.20	39.76	23.34	4.22	0.10
SHB1-3CH	7255.70–7357.89	6.87	28.02	39.78	21.60	3.72	0.00
SHB1-4H	7459.00–7561.96	5.89	25.25	40.26	24.37	4.22	0.00
SHB1-5H	7474.52–7576.19	6.32	25.45	39.48	24.31	4.44	0.00
SHB1-6H	7288.16–7399.75	6.24	26.30	40.21	23.19	4.06	0.00
SHB1-7H	7339.36–7456.00	5.31	24.00	40.48	25.58	4.64	0.00
SHB1-8H	7415.50–7571.64	5.78	24.72	39.66	24.97	4.85	0.00
SHB1-9	7372.74–7630.00	6.34	26.10	39.54	23.57	4.45	0.00
SHB1-10H	7229.50–8225.40	5.35	23.66	39.94	25.75	5.09	0.21
SHB3	7518.82-7891.26	3.62	19.96	39.95	29.42	6.87	0.18

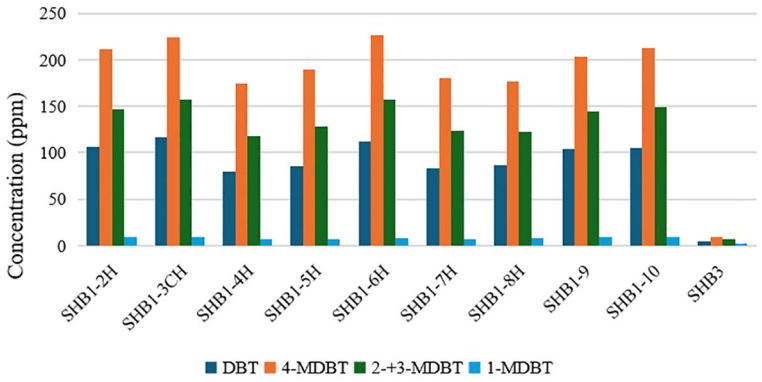

FIGURE 9
Concentration and distribution patterns of DBT and MDBTs.

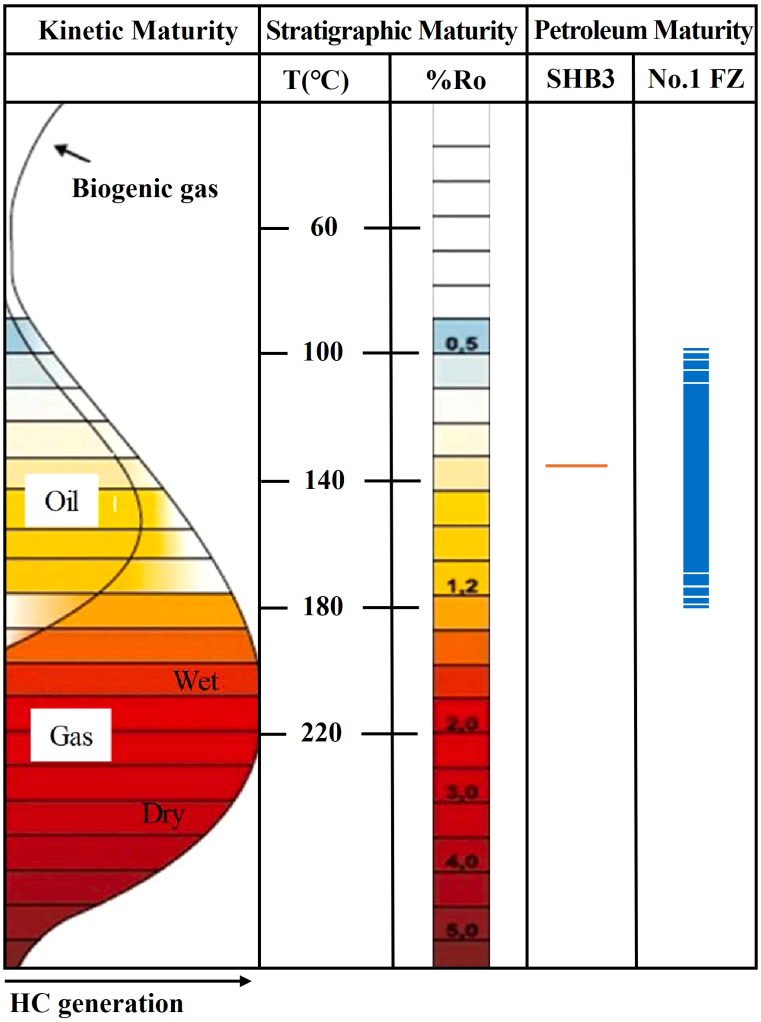

FIGURE 10
Thermal maturity model of reservoired petroleum in the No.1 and No.3 faults zones (modified after Huang et al., 2022). HC, hydrocarbon; FZ, fault zone.

petroleum in the sample trap and the lack of very late mature fractions. Such a scenario likely occurred when petroleum was expelled from source rocks and accumulated in the reservoirs of the No.3 fault zone within a limited oil generation interval. Alternatively, it could result from the opening and closing of strike-slip faults happened over a restricted geological timescale.

5.2 Implication for petroleum accumulation in Shunbei reservoirs

The Shunbei reservoirs are predominantly controlled by strike-slip faults (Figure 1a), as most wells with industrial petroleum production were located along these fault zones. Currently, petroleum in the Shunbei reservoirs is primarily sourced from Cambrian Yuertusi Formation, with strike-slip faults serving as pathways from the Cambrian source rocks to Ordovician reservoirs in the Shunbei area (Qi, 2021). The strike-slip faults in the Shunbei area are characterized by vertical stratification and plane segmentation within the fault zones, which is the major controlling factor of hydrocarbon accumulation (Liu, 2020).

These fault zones have recorded multiple stages of tectonic evolution, including the early Caledonian, middle Caledonian, late Caledonian-early Hercynian, late Hercynian, and Indosinian-Himalayan periods, contributing to the heterogeneity of hydrocarbon accumulation. For example, in the No.1 strike-slip fault zone, high-angle strike-slip faults and *en échelon* normal faults developed during the Paleozoic (Figure 11), while extensional faults were mainly formed during the Mesozoic–Cenozoic. The large-scale, pronounced segmentation and multi-phase activities in the No.1 fault zone facilitated multiple petroleum charging events. In contrast, the No.3 fault zone, characterized by smaller scale and less active tectonics (Figure 11), experienced petroleum charging within a narrower maturity interval.

The Tarim Basin exemplifies a region shaped by multi-phase tectonics and multiple petroleum charging periods, resulting in petroleum components that span a broad range of thermal maturities. Petroleum compositions are crucial for reconstructing

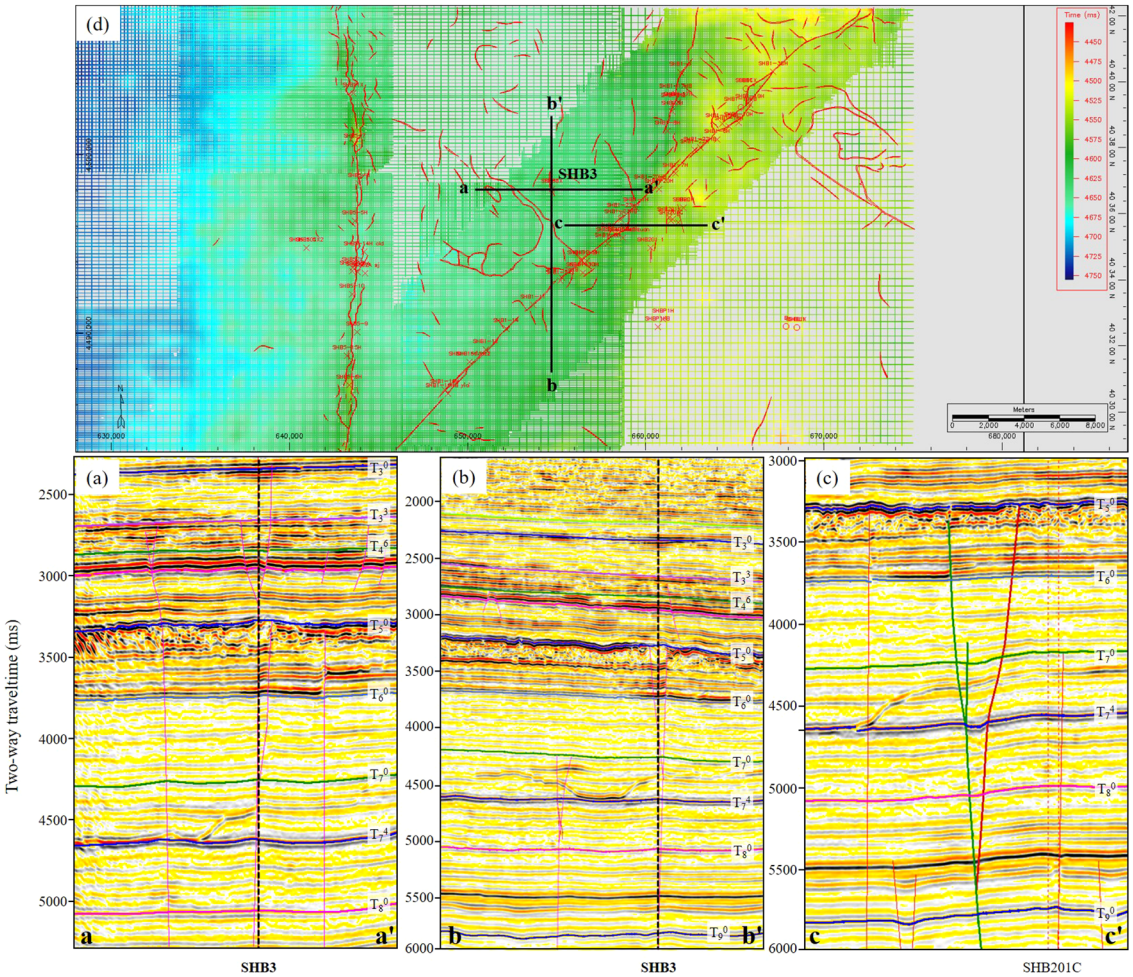

FIGURE 11
Seismic profiles of the Shunbei areas. **(a-c)** Fault interpretations of the cross sections with locations shown in Figure 11d. **(d)** The horizontal slice of T_7^4 interface.

hydrocarbon accumulation history in terms of petroleum generation, expulsion and charge processes. However, the presence of multiple source rocks and charging stages, coupled with a complex geologic history, poses challenges for deconvoluting source rock properties and expelled petroleum compositions.

The concept of an "instantaneous petroleum charge" offers a critical framework to establish correlations between reservoired oil and source rock maturity, particularly in cases where source rocks are difficult to obtain. The nature of instantaneous petroleum charge is equal to the stratigraphic maturity of source rock at a specific maturity level (Figure 10). Moreover, as petroleum is usually a mixture in the reservoirs, it is difficult to figure out the geochemical signature of individual petroleum charging episode which is the barrier to unravel hydrocarbon accumulation processes. By focusing on fraction maturity, this concept provides a powerful tool for deciphering the intricate petroleum accumulation histories and geological evolution of superimposed basins which could be a reference to identify more end members of instantaneous petroleum charge in reservoirs of worldwide scale.

6 Conclusions

Detailed organic geochemical analysis of oil samples from the No.1 and No.3 fault zones, has been conducted to unravel the petroleum charging history in the Shunbei reservoirs. Significant differences in biomarker and aromatic hydrocarbon distributions were observed between oil samples from these fault zones. SHB3 oil from the No.3 fault zone is characterized by low Ph/*n*-C_{18} and Pr/*n*-C_{17} ratios, an overwhelming predominance of high-carbon-number *n*-alkanes (> C_{19}) and an absence of steroid and terpenoid biomarkers. This suggests that SHB3 oil did not receive early-charged oil, in contrast to the oils from the No.1 fault zone. However, oil samples from the No.1 fault zone, exhibit higher concentrations of diamondoid hydrocarbons and more stable aromatic hydrocarbons, such as dibenzothiophene, indicating a higher proportion of mature fractions compared to SHB3 oil. This suggests that the reservoir associated with Well SHB3 has not undergone petroleum charging during the very late maturation stages. SHB3 oil spans a very narrow maturity range, which can be regarded as an end member for instantaneous petroleum charge. The end member of instantaneous petroleum charge in the Shunbei reservoirs offers valuable insights into the properties of hydrocarbons from individual petroleum charging period which sheds light on the complex hydrocarbon accumulation processes involving mixed maturities in superimposed basins.

Data availability statement

The original contributions presented in the study are included in the article/Supplementary Material. Further inquiries can be directed to the corresponding author.

Author contributions

QW: Funding acquisition, Validation, Writing – original draft, Writing – review & editing. HH: Funding acquisition, Investigation, Supervision, Validation, Writing – review & editing. TJ: Supervision, Writing – review & editing.

Funding

The author(s) declare that financial support was received for the research and/or publication of this article. This study was supported by the National Natural Science Foundation of China (Grant No.42473034, No.42406065), the SINOPEC Key Laboratory of Petroleum Accumulation Mechanisms (Grant No.33550007-22-ZC0613-0034), the National Key Research and Development Program of China (No.2024YFC2814702), the China Postdoctoral Science Foundation (Grant No.2023M733302) and the "CUG Scholar" Scientific Research Funds at China University of Geosciences (Wuhan) (Project No.2022096).

Acknowledgments

The author(s) acknowledge Prof. Steve Larter, Prof. Lloyd Snowdon and the other PRG members for their supervision and support of lab analysis. The authors thank Dr. Daqing Tang for his generosity in providing the seismic profiles of the Shunbei reservoirs. We thank the editor and reviewers for their reviews and constructive suggestions to improve the manuscript.

Conflict of interest

The authors declare that the research was conducted in the absence of any commercial or financial relationships that could be constructed as a potential conflict of interest.

Generative AI statement

The author(s) declare that no Generative AI was used in the creation of this manuscript.

Publisher's note

References

Alexander, R., Cumbers, K. M., and Kagi, R. I. (1986). Alkylbiphenyls in ancient sediments and petroleums. *Org. Geochem.* 10, 841–845. doi: 10.1016/S0146-6380(86)80021-3

Cumbers, K. M., and Alexander, R. (1987). Methylbiphenyl, ethylbiphenyl and dimethylbiphenyl isomer distributions in some sediments and crude oils. *Geochim. Cosmochim. Acta* 51, 3105–3111. doi: 10.1016/0016-7037(87)90121-9

Deng, S., Zhao, R., Kong, Q., Li, Y., and Li, B. (2022). Two distinct strike-slip fault networks in the Shunbei area and its surroundings, Tarim Basin: Hydrocarbon accumulation, distribution, and controlling factors. *Am. Assoc. Pet. Geol. Bull.* 106, 77–102. doi: 10.1306/07202119113

He, C., Huang, H., Wang, Q., and Li, Z. (2019). Correlation of maturity parameters derived from methylphenanthrenes and methyldibenzothiophenes in the Carboniferous source rocks from Qaidam Basin, NW China. *Geofluids*, 2019, 5742902. doi: 10.1155/2019/5742902

Horstad, I., and Larter, S.R. (1997). Petroleum migration, alteration, and remigration within Troll Field, Norwegian North Sea. *Am. Assoc. Pet. Geol. Bull.* 81, 222–248. doi: 10.1306/522B42F3-1727-11D7-8645000102C1865D

Huang, H., di Primio, R., Pedersen, J. H., Silva, R., Algeer, R., Ma, J., et al. (2022). On the determination of oil charge history and the practical application of molecular maturity markers. *Mar. Pet. Geol.* 139, 105586. doi: 10.1016/j.marpetgeo.2022.105586

Jia, C. (1997). *Tectonic characteristics and petroleum, Tarim Basin* (Beijing, China: Petroleum Industry Press).

Jiang, Z., Tang, D., Sha, X., Shen, X., Luo, S., Dong, K., et al. (2024). Structure and evolution of faults in central and Northern Parts of Tazhong Uplift,Tarim Basin. *Bull. Geol. Sci. Tech.* 43, 120–132. doi: 10.19509/j.cnki.dzkq.tb20220663

Larter, S. R., and Aplin, A. C. (1995). Reservoir geochemistry: methods, applications and opportunities. *Geol. Soc. Spec. Publ.* 86, 5–32. doi: 10.1144/GSL.SP.1995.086.01.02

Lerch, B., Karlsen, D. A., Matapour, Z., Seland, R., and Backer-Owe, K. (2016). Organic geochemistry of Barents Sea petroleum: Thermal maturity and alteration and mixing processes in oils and condensates. *J. Pet. Geol.* 39, 125–148. doi: 10.1111/jpg.12637

Liu, B. (2020). Analysis of the main controlling factors of oil and gas differential accumulation in the Shunbei area, Tarim Basin-taking Shunbei No. 1 and No. 5 strike-slip fault zones as examples. *China Pet. Explor.* 25, 83–95. doi: 10.3969/j.issn.1672-7703.2020.03.008

Liu, Y., Suppe, J., Cao, Y., Hao, F., Liu, Y., Wang, X., et al. (2023). Linkage and formation of strike-slip faults in deep basins and the implications for petroleum accumulation: A case study from the Shunbei area of the Tarim Basin, China. *Am. Assoc. Pet. Geol. Bull.* 107, 331–355. doi: 10.1306/11142220110

Liu, Y., Suppe, J., Cao, Y., Wu, K., Wang, J., Du, Y., et al. (2024). Strike-slip fault zone architecture and its effect on fluid migration in deep-seated strata: Insights from the Central Tarim Basin. *Basin Res.* 36, 12868. doi: 10.1111/bre.12868

Mukhopadhyay, P. K. (1994). Vitrinite reflectance as maturity parameter: petrographic and molecular characterization and its applications to basin modeling. *ACS Symp. Ser. Am. Chem. Soc.* 570, 1–24. doi: 10.1021/bk-1994-0570.ch001

Qi, L. (2021). Structural characteristics and storage control function of the Shun I fault zone in the Shunbei region, Tarim Basin. *J. Pet. Sci. Eng.* 203, 108653. doi: 10.1016/j.petrol.2021.108653

Qiu, H., Deng, S., Cao, Z., Yin, T., and Zhang, Z. (2019). The evolution of the complex anticlinal belt with crosscutting strike-slip faults in the central Tarim Basin, NW China. *Tectonics* 38, 2087–2113. doi: 10.1029/2018TC005229

Radke, M., Welte, D. H., and Willsch, H. (1982b). Geochemical study on a well in the Western Canada Basin: relation of the aromatic distribution pattern to maturity of organic matter. *Geochim. Cosmochim. Acta* 46, 1–10. doi: 10.1016/0016-7037(82)90285-X

Radke, M., Welte, D. H., and Willsch, H. (1986). Maturity parameters based on aromatic hydrocarbons: Influence of the organic matter type. *Org. Geochem.* 10, 51–63. doi: 10.1016/0146-6380(86)90008-2

Radke, M., Willsch, H., Leythaeuser, D., and Teichmüller, M. (1982a). Aromatic components of coal: relation of distribution pattern to rank. *Geochim. Cosmochim. Acta* 46, 1831–1848. doi: 10.1016/0016-7037(82)90122-3

Seifert, W. K., and Moldowan, J. M. (1978). Applications of steranes, terpanes and monoaromatics to the maturation, igration and source of crude oils. *Geochem. Cosmochim. Acta* 42, 77–95. doi: 10.1016/0016-7037(78)90219-3

Tissot, B. P., Pelet, R., and Ungerer, P. H. (1987). Thermal history of sedimentary basins, maturation indices, and kinetics of oil and gas generation. *Am. Assoc. Pet. Geol. Bull.* 71, 1445–1466. doi: 10.1306/703C80E7-1707-11D7-8645000102C1865D

Ungerer, P. H., and Pelet, R. (1987). Extrapolation of the kinetics of oil and gas formation from laboratory experiments to sedimentary basins. *Nature* 327, 52–54. doi: 10.1038/327052a0

van Aarssen, B. G., Bastow, T. P., Alexander, R., and Kagi, R. I. (1999). Distributions of methylated naphthalenes in crude oils: Indicators of maturity, biodegradation and mixing. *Org. Geochem.* 30, 1213–1227. doi: 10.1016/S0146-6380(99)00097-2

Wang, Q., Huang, H., Chen, H., and Zhao, Y. (2020). Secondary alteration of ancient Shuntuoguole oil reservoirs, Tarim Basin, NW China. *Mar. Pet. Geol.* 111, 202–218. doi: 10.1016/j.marpetgeo.2019.08.013

Wang, Q., Huang, H., He, C., Li, Z., and Zheng, L. (2022). Methylation and demethylation of naphthalene homologs in highly thermal mature sediments. *Org. Geochem.* 163, 104343. doi: 10.1016/j.orggeochem.2021.104343

Wang, Q., Huang, H., Li, Z., and Li, Z. (2019). Novel thermal maturity parameters derived from alkylbiphenyls and alkyldiphenylmethanes. *Energ. Fuel* 33, 8491–8502. doi: 10.1021/acs.energyfuels.9b02084

Wang, Q., Huang, H., Li, Z., Ma, Y., Zeng, J., and Larter, S. (2021a). Geochemical significance of β-carotane in lacustrine oils from the Shahejie Formation of the Dongying Depression, eastern China. *Org. Geochem.* 156, 104241. doi: 10.1016/j.orggeochem.2021.104241

Wang, Q., Huang, H., Sun, J., Huang, J., and Jiang, T. (2025). Limitations of diamondoids in the quantitative evaluation of petroleum cracking in ultra-deep carbonate reservoirs of the Shunbei area, Tarim Basin. *Front. Mar. Sci.* 12, 1578161. doi: 10.3389/fmars.2025.1578161

Wang, Q., Huang, H., and Zheng, L. (2021b). Thermal maturity parameters derived from tetra-, penta-substituted naphthalenes and organosulfur compounds in highly mature sediments. *Fuel* 288, 119626. doi: 10.1016/j.fuel.2020.119626

Wilhelms, A., and Larter, S. (2004). Shaken but not always stirred. Impact of petroleum charge mixing on reservoir geochemistry. *Geol. Soc. Spec. Publ.* 237, 27–35. doi: 10.1144/GSL.SP.2004.237.01.03

Wu, W., Chen, H., Su, A., Wang, Y., Zhu, Z., He, J., et al. (2023). The contribution of petroleum charging episodes to different strike-slip fault zones in the Shunbei area, the Tarim Basin, NW China. *Energies* 16, 579. doi: 10.3390/en16020579

Wu, G., Gao, L., Zhang, Y., Ning, C., and Xie, E. (2019). Fracture attributes in reservoir-scale carbonate fault damage zones and implications for damage zone width and growth in the deep subsurface. *J. Struct. Geol.* 118, 181–193. doi: 10.1016/j.jsg.2018.10.008

Yang, P., Liu, K., Evans, N. J., Zhang, S., Li, Z., Su, J., et al. (2024). Petroleum accumulation history of deeply buried carbonate reservoirs in the northern Tarim Basin, northwestern China. *Am. Assoc. Pet. Geol. Bull.* 108, 1193–1229. doi: 10.1306/06212321210

Zhang, S., and Huang, H. (2005). Geochemistry of Palaeozoic marine petroleum from the Tarim Basin, NW China: Part 1. Oil family classification. *Org. Geochem.* 36, 1204–1214. doi: 10.1016/j.orggeochem.2005.01.013

Zhang, S., Huang, H., Su, J., Zhu, G., Wang, X., and Larter, S. (2014). Geochemistry of Paleozoic marine oils from the Tarim Basin, NW China. Part 4: Paleobiodegradation and oil charge mixing. *Org. Geochem.* 67, 41–57. doi: 10.1016/j.orggeochem.2013.12.008

Zhang, S., Huang, H., Xiao, Z., and Liang, D. (2005). Geochemistry of Palaeozoic marine petroleum from the Tarim Basin, NW China. Part 2: maturity assessment. *Org. Geochem.* 36, 1215–1225. doi: 10.1016/j.orggeochem.2005.01.014

Zhang, S., Su, J., Wang, X., Zhu, G., Yang, H., Liu, K., et al. (2011). Geochemistry of Palaeozoic marine petroleum from the Tarim Basin, NW China: Part 3. Thermal cracking of liquid hydrocarbons and gas washing as the major mechanisms for deep gas condensate accumulations. *Org. Geochem.* 42, 1394–1410. doi: 10.1016/j.orggeochem.2011.08.013

Zhu, G., Zhang, S., Su, J., Huang, H., Yang, H., Gu, L., et al. (2012). The occurrence of ultra-deep heavy oils in the Tabei Uplift of the Tarim Basin, NW China. *Org. Geochem.* 52, 88–102. doi: 10.1016/j.orggeochem.2012.08.012